J Biol Inorg Chem (2009) 14:559–571
DOI 10.1007/s00775-009-0470-3

ORIGINAL PAPER

# Effect of metal ion substitutions in anticoagulation factor I from the venom of *Agkistrodon acutus* on the binding of activated coagulation factor X and on structural stability

**Xiaolong Xu · Liyun Zhang · Dengke Shen · Hao Wu · Lili Peng · Jiehua Li**

Received: 2 September 2008 / Accepted: 11 January 2009 / Published online: 31 January 2009


**Abstract** Anticoagulation factor I (ACF I) isolated from the venom of *Agkistrodon acutus* is an activated coagulation factor X (FXa)-binding protein that binds in a $Ca^{2+}$-dependent fashion with marked anticoagulant activity. The thermodynamics of the binding of alkaline earth metal ions to ACF I and the effects of alkaline earth metal ions on the guanidine hydrochloride (GdnHCl)-induced unfolding of ACF I and the binding of ACF I to FXa were studied by isothermal titration calorimetry, fluorescence, circular dichroism, and surface plasmon resonance, respectively. The results indicate that the ionic radii of the cations occupying $Ca^{2+}$-binding sites in ACF I crucially affect the binding affinity of ACF I for alkaline earth metal ions as well as the structural stability of ACF I against GdnHCl denaturation. $Sr^{2+}$ and $Ba^{2+}$, with ionic radii larger than the ionic radius of $Ca^{2+}$, can bind to $Ca^{2+}$-free ACF I (apo-ACF I), while $Mg^{2+}$, with an ionic radius smaller than that of $Ca^{2+}$, shows significantly low affinity for the binding to apo-ACF I. All bindings of $Ca^{2+}$, $Sr^{2+}$, and $Ba^{2+}$ ions in two sites of ACF I are mainly enthalpy-driven and the entropy is unfavorable for them. $Sr^{2+}$-stabilized ACF I exhibits slightly lower resistance to GdnHCl denaturation than $Ca^{2+}$–ACF I, while $Ba^{2+}$-stabilized ACF I exhibits much lower resistance to GdnHCl denaturation than $Ca^{2+}$–ACF I. $Mg^{2+}$ and $Sr^{2+}$, with ionic radii close to that of $Ca^{2+}$, can bind to FXa and therefore also induce the binding of ACF I to FXa, whereas $Ba^{2+}$, with a much larger ionic radius than $Ca^{2+}$, cannot support the binding of ACF I with FXa. Our observations suggest that bindings of $Ca^{2+}$, $Sr^{2+}$, and $Ba^{2+}$ ions in two sites of ACF I increase the structural stability of ACF I, but these bindings are not essential for the binding of ACF I with FXa, and that the binding of $Mg^{2+}$, $Ca^{2+}$, and $Sr^{2+}$ ions to FXa may be essential for the recognition between FXa and ACF I.

**Keywords** Anticoagulation factor I · Alkaline earth metal ions · Unfolding · Isothermal titration calorimetry · Fluorescence

**Abbreviations**

| | |
|---|---|
| ACF I | Anticoagulation factor I |
| apo-ACF I | $Ca^{2+}$-free ACF I |
| CD | Circular dichroism |
| FIX | Coagulation factor IX |
| FIXa | Activated coagulation factor IX |
| FX | Coagulation factor X |
| FXa | Activated coagulation factor X |
| GdnHCl | Guanidine hydrochloride |
| Gla | γ-Carboxyglutamic acid |
| ITC | Isothermal titration calorimetry |
| IX/X-bp | Coagulation factor IX/coagulation factor X binding protein |
| PAGE | Polyacrylamide gel electrophoresis |
| SPR | Surface plasmon resonance |
| Tris | Tris(hydroxymethyl)aminomethane |
| X-bp | Coagulation factor X binding protein |

X. Xu (✉) · L. Zhang · D. Shen · H. Wu · L. Peng
Department of Chemistry,
University of Science and Technology of China,
230026 Hefei,
People's Republic of China
e-mail: xuxl@ustc.edu.cn

J. Li
Department of Geriatric Cardiology,
The First Affiliated Hospital of Anhui Medical University,
230022 Hefei,
People's Republic of China

## Introduction

Coagulation factor IX (FIX) and coagulation factor X (FX) are two pivotal participants in the blood coagulation cascade, in which the two factors are sequentially activated, leading to the formation of insoluble fibrin clots from the soluble fibrinogen [1]. A family of FIX/FX binding proteins (IX/X-bps) has been found from snake venoms [2–6]. The proteins of this family have high homologous sequences, and form 1:1 complexes with FIX/activated FIX (FIXa) or FX/activated FX (FXa) and prolong the clotting time [7–9]. IX/X-bps bind with the $\gamma$-carboxyglutamic acid (Gla) domain of FIX or FX in a $Ca^{2+}$-dependent manner [10]. The structures of habu IX/X-bp [11], habu FIX-binding protein [12] from habu snake venom, and *Deinagkistrodon* FX-binding protein (*Deinagkistrodon* X-bp) [10] from *Deinagkistrodon* venom are very similar. In addition, the complex of *Deinagkistrodon* X-bp with the Gla domain of FX has been determined [10].

It was reported that $Sr^{2+}$ and $Mg^{2+}$ ions could be substituted for $Ca^{2+}$ ions in *Bothrops jararaca* IX/X-bp, an anticoagulant protein from the venom of *B. jararaca*, in binding of FIX, but the binding of *B. jararaca* IX/X-bp to FX had an absolute requirement for $Ca^{2+}$ ions [2]. Similarly, $Sr^{2+}$ ions could substitute $Ca^{2+}$ ions in *Echis carinatus leucogaster* IX/X-bp from the venom of *E. carinatus leucogaster* for inducing the protein to bind FIX. However, $Sr^{2+}$ ions were not able to substitute $Ca^{2+}$ ions in the binding of *E. carinatus leucogaster* IX/X-bp to FX [4].

Anticoagulation factor I (ACF I) purified from the venom of *Agkistrodon acutus* is a member of the family of IX/X-bps, because it forms a 1:1 complex with FXa in a $Ca^{2+}$-dependent fashion, and thereby blocks the amplification of the coagulation cascade [13, 14]. ACF I, as a naturally occurring anticoagulant, is devoid of hemorrhagic and lethal activities, which may be useful both as a basis for designing anticoagulant drugs and as a convenient tool in exploration of the complex mechanisms of the coagulation cascade. ACF I has an amino acid sequence highly similar to that of *Deinagkistrodon* X-bp, with only residue Asn-70 in the $\beta$ chain of ACF I being replaced by Lys-70 in *Deinagkistrodon* X-bp [15], and has a structure typical of IX/X-bps (Protein Data Bank code 1wt9). As shown in Fig. 1, ACF I is a heterodimer protein consisting of two homologous chains with a similar topology structure linked with a disulfide bond. Each chain has one $Ca^{2+}$-binding site. One of them is formed by the oxygen atoms of Ser-41, Glu-43, Glu-47, and Glu-128 in the A chain, and the other site is formed by the oxygen atoms of Ser-41, Gln-43, Glu-47, and Glu-120 in the B chain. Our previous studies showed that $Ca^{2+}$ ions not only increased the structural stability of ACF I against guanidine hydrochloride (GdnHCl) denaturation, but also induced a refolding of ACF I [16].

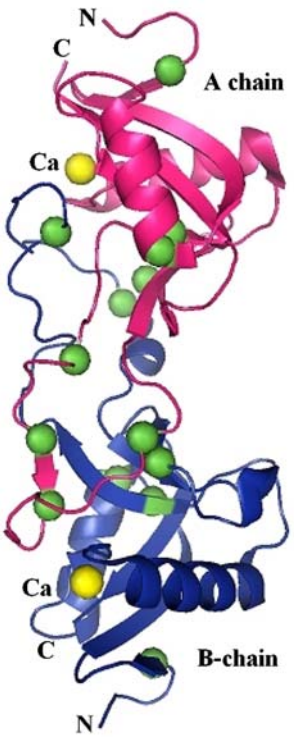


**Fig. 1** Ribbon model of the heterodimer polypeptide chains of anticoagulation factor I (ACF I). The $Ca^{2+}$ ions and Trp residues are indicated as *yellow balls* and *green balls*, respectively. The picture was drawn with Protein Data Bank file 1wt9

Despite the structural and metal ion substitution studies for several IX/X-bps, the thermodynamic properties of IX/X-bps with metal ions and the effect of metal ion substitutions in IX/X-bps on their structural stability remain unclear. To complement information gained from structural studies, we used thermodynamic and energetic approaches to investigate metal ion binding and metal-ion-induced stabilization for ACF I. Both $Ca^{2+}$ ions in ACF I are coordinated by side-chain oxygen atoms (Protein Data Bank code 1wt9). Alkaline earth metal ions, such as $Mg^{2+}$, $Ca^{2+}$, $Sr^{2+}$, and $Ba^{2+}$, are all hard acids and have high affinity for oxygen atoms. These alkaline earth metal ions have the same positive charge but different ionic radii. We expected that the thermodynamic and energetic analysis of the substitutions of $Mg^{2+}$, $Sr^{2+}$, and $Ba^{2+}$ for $Ca^{2+}$ ions in ACF I would be useful for improving our understanding of the effects of metal ion radii on the structural stability and function of ACF I. Here, we describe the thermodynamic characterization of the binding of ACF I with $Ca^{2+}$, $Mg^{2+}$, $Sr^{2+}$, and $Ba^{2+}$ by isothermal titration calorimetry (ITC). In addition, the effects of the metal ion substitutions on the binding of ACF I with FXa as well as on the GdnHCl-induced unfolding and metal-ion-induced partial refolding behavior of ACF I have been studied.

Metal ions are known to be essential to the structure and function of enzymes and some proteins [17–19]. Recently,

the metal ion selectivity in proteins and the effects of metal ions on the structure and function of proteins have received considerable attention. The metal ion selectivity in proteins is known to be based on the ionic charge [20], radius [21], and binding geometry [22]. It has been shown that metal-ion-induced conformational changes in several enzymes lead to stabilization or destabilization of the proteins [17, 23–30].

The present investigation suggests that the binding of ACF I to FXa does not have an absolute requirement for $Ca^{2+}$ ions. $Mg^{2+}$ and $Sr^{2+}$ ions can induce the binding of ACF I to FXa and the metal ionic radii have significant effects on the metal-ion-induced structural stability of ACF I against GdnHCl denaturation as well as on the GdnHCl-induced unfolding and metal-ion-induced partial refolding behavior of ACF I. These findings provide new insights into the metal selectivity in ACF I as well as the role of $Mg^{2+}$ in the anticoagulation of ACF I.

## Materials and methods

### Materials

Lyophilized venom powder was provided by the TUN-XI Snakebite Institute (Anhui, People's Republic of China). GdnHCl (ultrapure) was obtained from Sigma Chemical Company (St Louis, MO, USA). Chelex-100 was purchased from Bio-Rad Laboratories (Richmond, CA, USA). Activated bovine FX (FXa) was a generous gift from Zhao Chao, Research Center for Eco-Environmental Sciences, Chinese Academy of Sciences. All other reagents were of analytical reagent grade.

### Preparation of protein and solution

ACF I and $Ca^{2+}$-free ACF I (apo-ACF I) were prepared by the method described previously [13, 16]. $Sr^{2+}$–ACF I and $Ba^{2+}$–ACF I were prepared by incubation of apo-ACF I in 0.01 M tris(hydroxymethyl)aminomethane (Tris) buffer (pH 7.6) with 1 mM $Sr^{2+}$ and 1 mM $Ba^{2+}$, respectively, for 30 min at 4 °C. ACF I concentration was calculated from the absorption coefficient ($A^{1\%}_{1cm} = 31$) at 280 nm and the molecular weight ($M_r = 29{,}245$). The solutions of $Mg^{2+}$, $Ca^{2+}$, $Sr^{2+}$, and $Ba^{2+}$ ions were prepared from $MgCl_2$, $CaCl_2$, $SrCl_2$, and $BaCl_2$ in Milli-Q water, respectively, and standardized by titration with standard EDTA solution. The pH values of metal ion solutions were adjusted to 6.0 with HCl or NaOH. The Tris buffer used was freed from any possible contamination of multivalent cations by passage through a column (25 cm × 3 cm) of Chelex-100. Because ACF I exhibited the highest binding affinity for FXa at pH 7.6, Tris buffer at pH 7.6 was used throughout. GdnHCl was determined to be metal-free by extraction with dithizone (6 mg/l) in carbon tetrachloride. All utensils used during the experiments were made metal-free by soaking them in 2 M $HNO_3$ for 24 h, and then by extensively rinsing them with Milli-Q purified water.

### Dialysis

Apo-ACF I solution (70 μM) was dialyzed against 0.02 M Tris–HCl buffer (pH 7.6) containing 100 μM $Mg^{2+}$, $Sr^{2+}$, or $Ba^{2+}$ for 24 h at 4 °C, and then the concentrations of metal ion in the sample and buffer solutions, respectively, were measured by a PLASMA-100 inductively coupled plasma atomic emission spectrometer.

### ITC measurements

ITC experiments were carried out at 25 °C using a MicroCal VP-ITC microcalorimeter (MicroCal), as described by Smith and Windsor [31]. All buffers and solutions were degassed immediately before each titration. The reference cell was filled with buffer. The sample cell was filled with 12 μM ACF I and 20 mM Tris–HCl buffer pH 7.6, and the titration syringe was filled with 0.6 mM metal ion solution in 20 mM Tris–HCl, pH 7.6. The system was equilibrated at 25 °C with stirring at 307 rpm prior to the addition of 240 μl of 0.6 mM metal ion solution. The protein in the 1.468-ml calorimeter cell was titrated with metal ion solution by 30 successive automatic injections of 8 μl each. Before termination of the experiment, the thermal power was allowed to return to the level matching the original baseline, indicating complete reaction. Aliquots of the same concentrated metal ion solution were injected into the buffer solution (without the protein) in a separate ITC run to subtract the heat of dilution. The area under the baseline was integrated and divided by the total amount of metal ion added to the cell to determine the molar enthalpy of the reaction.

The thermodynamic parameters $N$ (stoichiometry), $K_A$ (association constant), and $\Delta H$ (enthalpy change) were obtained by nonlinear least-squares fitting of experimental data using a two sequential sites model of the Origin software package (version 7.0) provided with the instrument. The free energy of binding ($\Delta G$) and the entropy change ($\Delta S$) were obtained using the following equations:

$$\Delta G = -\mathrm{RT}\ln K_A, \quad (1)$$

$$\Delta G = \Delta H - T\Delta S. \quad (2)$$

The affinity of a metal ion for protein is given as the dissociation constant ($K_D = 1/K_A$). For each metal ion–protein interaction, three titrations were performed. Titration data were analyzed independently, and the thermodynamic values obtained were averaged.

### Electrophoresis

Native polyacrylamide gel electrophoresis (PAGE) was used for analysis of the effects of metal ions on the binding of ACF I and FXa. It was performed in 2.5% stacking gel at pH 6.7 and 7.5% separation gel at pH 8.9. A pH 8.3 Tris–Gly solution was used as the electrolyte buffer solution. Both the sample solution as well as the electrolyte buffer solution, and the separation gel as well as the stacking gel contained 1 mM $Mg^{2+}$, $Sr^{2+}$, or $Ba^{2+}$ to keep ACF I in the presence of 1 mM $Mg^{2+}$, $Sr^{2+}$, or $Ba^{2+}$ in the PAGE process.

### Surface plasmon resonance

Surface plasmon resonance (SPR) measurements were performed at 25 °C using a Biacore 3000 instrument. Sensor surfaces were pretreated and then normalized by standard Biacore protocols [32]. FXa was diluted in immobilization buffer (1 μM, in 10 mM sodium acetate, pH 5.0) and immobilized onto one flow cell of a CM5 chip. For coupling of FXa to CM5 sensor surfaces, the surfaces were activated with a 2-min pulse of *N*-ethyl-*N*-(dimethylaminopropyl)carbodiimide/*N*-hydroxysuccinimide (10 μl/min in phosphate-buffered saline), followed by injection of the protein, and then deactivated by a 2-min pulse of ethanolamine (pH 8.5, 10 μl/min). ACF I of various concentrations (0.31–10 μM) in 0.02 M Tris–HCl (pH 7.6) was injected over the surface (10 μl/min, 20-μl injection with 300-s wash delay). The surface was regenerated between analyte injections with 1 M NaCl and 1 mM EDTA (50 μl at 20 μl/min). The data were transferred into BiaEvaluation 4.1 and fitted using an equilibrium binding analysis.

### Steady-state fluorescence measurements

All fluorescence measurements were performed using a Shimadzu RF-5000 spectrofluorometer using a 10-mm quartz cuvette. The sample temperature was kept at 25.0 °C by a circulating water bath. In all experiments, the samples were excited at 295 nm, and the bandwidths for excitation and emission were both set to 2 nm. Each spectrum is the average of three consecutively acquired spectra. All spectra were corrected by subtracting the spectrum of the blank, lacking the protein but otherwise identical to the sample.

### Circular dichroism measurements

Circular dichroism (CD) measurements were carried out with a JASCO J-720 spectropolarimeter. All the CD measurements were made at 25 °C with a thermostatically controlled cell holder. Far-UV CD spectra were collected with a scan speed of 20 nm/min and a response time of 1 s, at a protein concentration of 0.10 mg/ml, in quartz cells of 1-mm path length. The values obtained were normalized by subtracting the baseline recorded for the buffer having same concentration of salts under similar conditions. The data were expressed as mean residue ellipticity [$\theta$] in degrees centimeter squared per decimole, which is defined as $[\theta] = 100\theta_{obs}(lc)^{-1}$, where $\theta_{obs}$ is the observed ellipticity in degrees, $c$ is the concentration in residue moles per liter, and $l$ is the length of the light path in centimeters.

### Denaturation experiments

Solutions for the denaturation experiments were prepared from stock solutions of protein and GdnHCl prepared in 20 mM Tris–HCl, pH 7.6. The concentration of the concentrated stock solution of GdnHCl was determined refractometrically [33]. In accordance with the method described by Muzammil et al. [34], in denaturation experiments, to a stock protein solution different volumes of the buffer were added first and the denaturant was added last so as to get the desired concentration of denaturant. The final solution mixture for the denaturation experiment was incubated for 1 h at 25 °C before fluorescence measurements. Unfolding curves were analyzed using either two-state (N ↔ D) or three-state (N ↔ I ↔ D) mechanisms as described in detail previously [16, 35, 36]. The thermodynamic and spectroscopic parameters were optimized in global fits by nonlinear least-squares analysis using the Marquardt–Levenburg algorithm in a routine software [37].

### Partial refolding kinetic measurements

For the partial refolding kinetic measurements, 1 ml of the sample solution was continuously excited at 295 nm and the emission intensity was collected at 338 nm with a response time of 1.0 s. The data were collected in the time scan mode after the partial refolding process had been initiated by adding 2 μl of 0.5 M metal ions and collection continued for at least 40 min.

## Results

### Metal ion binding assessed by dialysis

Holo-ACF I contains two $Ca^{2+}$ ions. To determine the binding of apo-ACF I ($Ca^{2+}$-free ACF I) with the metal ions of group IIA, an equilibrium dialysis was carried out. After extensive dialysis of 70 μM apo-ACF I against 100 μM $Mg^{2+}$, $Sr^{2+}$, and $Ba^{2+}$ in 0.02 M Tris–HCl buffer

(pH 7.6), the values of $c_{Mg(II)}/c_{ACF\ I}$, $c_{Sr(II)}/c_{ACF\ I}$, and $c_{Ba(II)}/c_{ACF\ I}$ were determined to be 0.11 ± 0.05, 1.91 ± 0.06, and 1.76 ± 0.09, respectively, by inductively coupled plasma atomic emission spectrometry. This result indicates that one ACF I molecule binds with two $Sr^{2+}$ ions or two $Ba^{2+}$ ions, but $Mg^{2+}$ ions have a markedly low binding affinity for ACF I.

## Metal ion binding assessed by ITC

ITC was used to quantify metal ion binding to apo-ACF I. Figure 2 shows representative thermograms of $Mg^{2+}$, $Ca^{2+}$, $Sr^{2+}$, and $Ba^{2+}$ titrated into apo-ACF I in 20 mM Tris, pH 7.6. As shown in Fig. 2a, the heat liberated at each injection is nearly zero and the overall ITC profile does not indicate an obvious binding pattern, which further suggests that $Mg^{2+}$ ions have significantly low binding affinity for ACF I. The exothermic evolution of heat upon $Ca^{2+}$, $Sr^{2+}$, and $Ba^{2+}$ injections shown in the upper panels in Fig. 2b–d illustrates $Ca^{2+}$, $Sr^{2+}$, and $Ba^{2+}$ binding to apo-ACF I, respectively. A good fit to the data for each calorimetric titration can be achieved using a two sequential sites model in the Origin software package provided with the MicroCal titration calorimeter, and the average best-fit values of the thermodynamic parameters ($K_A$, $\Delta G$, $\Delta H$, and $\Delta S$) are summarized in Table 1. The ITC data clearly demonstrate that two $Ca^{2+}$ ions bind to the protein. Both high-affinity and low-affinity sites are exothermic in nature. The negative $\Delta H$ and $\Delta S$ values of the binding interactions between apo-ACF I and $Ca^{2+}$ ions in both sites indicate that both binding types are mainly enthalpy-driven and the entropy is unfavorable for them. Similar results were obtained for the binding of apo-ACF I with $Sr^{2+}$ and $Ba^{2+}$ ions. ACF I has a relatively strong site and a relatively weak affinity site for either $Sr^{2+}$ ions or $Ba^{2+}$ ions. Both high-affinity and low-affinity sites are exothermic for either $Sr^{2+}$ ions or $Ba^{2+}$ ions. All binding types for both $Sr^{2+}$ and $Ba^{2+}$ ions in two sites are mainly enthalpy-driven and the entropy is unfavorable for them.

## Effects of metal ions on the binding of ACF I to FXa

Native PAGE was used to analyze the effects of metal ion substitutions on the binding of ACF I to FXa. As shown in Fig. 3a, in the presence of 1 mM $Mg^{2+}$, the mixture of apo-ACF I and FXa (1:1 mol/mol) produced one band (Fig. 3a, lane 2) and the band corresponding to apo-ACF I disappeared, suggesting that apo-ACF I should form a complex with FXa in the presence of 1 mM $Mg^{2+}$. As shown in Fig. 3b, a new band with a slower migration ratio was observed on the gel when FXa was mixed with excess $Sr^{2+}$–ACF I (1:2 mol/mol) in the presence of 1 mM $Sr^{2+}$, while the FXa band disappeared and the $Sr^{2+}$–ACF I band was weakened, indicating that with excess $Sr^{2+}$–ACF I all FXa should bind with $Sr^{2+}$–ACF I in the presence of 1 mM $Sr^{2+}$. In contrast, as shown in Fig. 3c, no new bands appeared when FXa was incubated with $Ba^{2+}$–ACF I (1:1 mol/mol) in the presence of 1 mM $Ba^{2+}$, suggesting that $Ba^{2+}$–ACF I should not bind with FXa.

SPR spectroscopy was used to further analyze the effects of metal ion on the binding of ACF I to FXa. Figure 4 illustrates association and dissociation curves for apo-ACF I interacting with FXa in the presence of 1 mM $Mg^{2+}$, $Ca^{2+}$, $Sr^{2+}$, or $Ba^{2+}$. Apo-ACF I shows specific binding with FXa in the presence of 1 mM $Mg^{2+}$, $Ca^{2+}$, or $Sr^{2+}$; however, no obvious binding between apo-ACF I and FXa was observed in the presence of 1 mM $Ba^{2+}$. The kinetic parameters, on-rate ($k_{on}$), off-rate ($k_{off}$), association constant ($K_A$), and dissociation constant ($K_D$), were obtained for each interaction by a fit of the data to a 1:1 Langmuir model and are shown in Table 2. Apo-ACF I binds to FXa with higher affinity in the presence of 1 mM $Mg^{2+}$ or $Ca^{2+}$, and with lower affinity in the presence of 1 mM $Sr^{2+}$. These results further confirm that all $Mg^{2+}$, $Ca^{2+}$, and $Sr^{2+}$ ions can induce the binding of ACF I to FXa, but $Ba^{2+}$ is ineffective in inducing this binding.

## Effects of metal ions on GdnHCl-induced unfolding of ACF I

Previously, we showed that the GdnHCl-induced unfolding of apo-ACF I follows a two-state mechanism with $\Delta G^0$ of 4.50 ± 0.08 kcal/mol, while GdnHCl-induced denaturation of $Ca^{2+}$–ACF I follows a four-state mechanism with $\Delta G^0_{total}$ of 6.01 ± 0.09 kcal/mol [16]. Fluorescence spectroscopy is a powerful technique to monitor unfolding transitions [38, 39].; therefore, the intrinsic fluorescence of Trp residues in ACF I was used to investigate the effects of $Mg^{2+}$, $Sr^{2+}$, and $Ba^{2+}$ ions on the GdnHCl-induced unfolding behavior of ACF I. As shown in Fig. 5, GdnHCl-induced denaturation of apo-ACF I in the presence of 1 mM $Mg^{2+}$ was found to be a two-state process with no detectable intermediate state(s). The unfolding transition curve of apo-ACF I in the presence of 1 mM $Mg^{2+}$ is very similar to that of apo-ACF I in the absence of $Mg^{2+}$ [16]. The thermodynamic parameters for the transition of GdnHCl-induced unfolding of apo-ACF I in the presence of 1 mM $Mg^{2+}$ were obtained by nonlinear least-squares analysis. As shown in Table 3, the $\Delta G^0$, $C_m$, and $m$ values obtained for the GdnHCl-induced unfolding transition of apo-ACF I in the presence of 1 mM $Mg^{2+}$ are also very similar to those obtained for apo-ACF I in the absence of $Mg^{2+}$ [16], indicating that $Mg^{2+}$ ions do not affect GdnHCl-induced unfolding of apo-ACF I.

As shown in Fig. 5, GdnHCl-induced denaturation of $Sr^{2+}$–ACF I was found to be a three-state process with

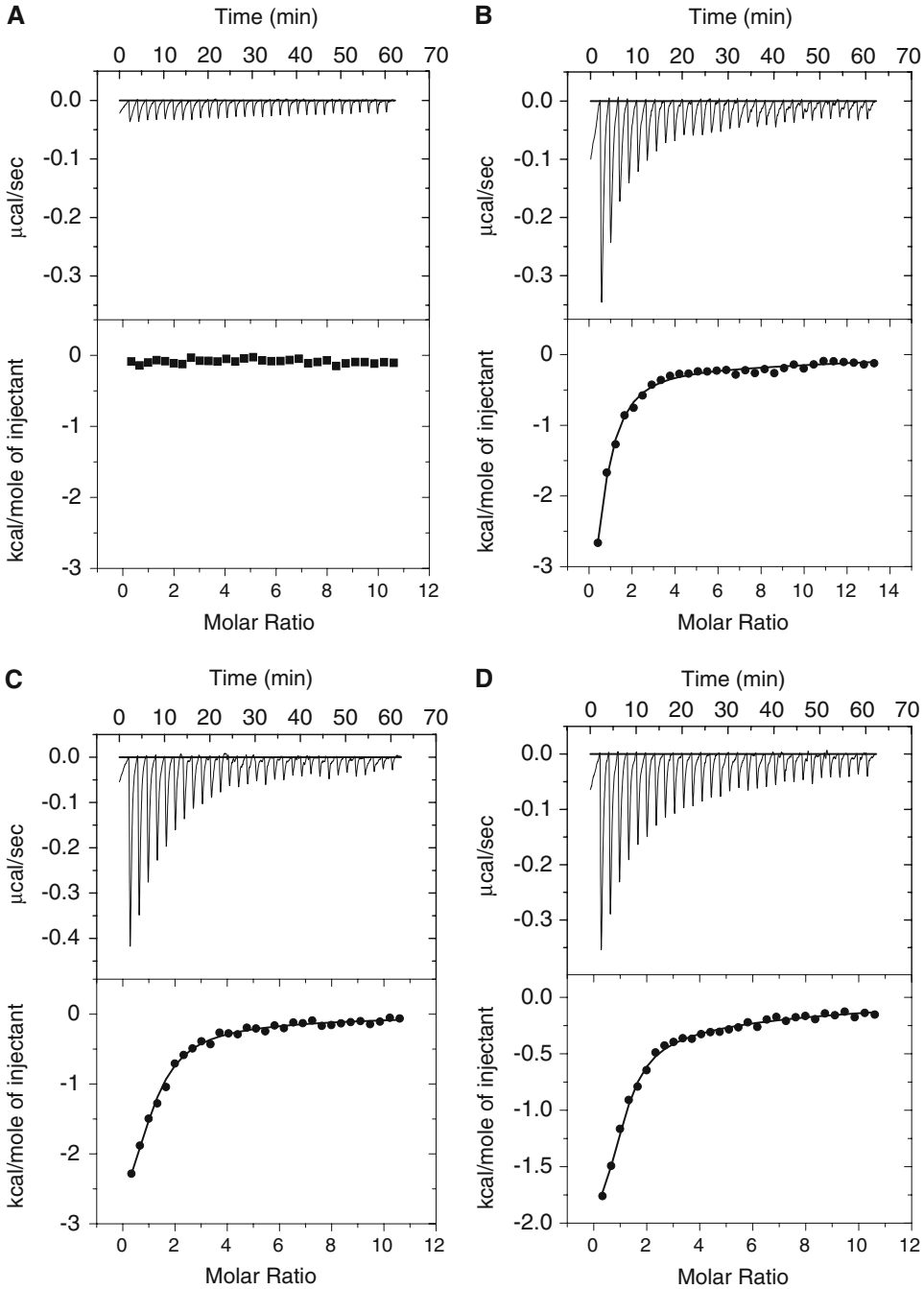


**Fig. 2** Isothermal titration calorimetry (ITC) measurements of $Mg^{2+}$ (**a**), $Ca^{2+}$ (**b**), $Sr^{2+}$ (**c**), and $Ba^{2+}$ (**d**) binding to $Ca^{2+}$-free ACF I (apo-ACF I). Raw ITC data for injecting 0.6 mM alkaline earth metal ions in 20 mM tris(hydroxymethyl) aminomethane (Tris)–HCl, pH 7.6 into 12 μM ACF I in the same buffer at 25 °C (*upper panels*). Normalized ITC data for titrations versus molar ratio of metal ion to apo-ACF I (*lower panels*). Data analysis using the Origin 7.5 software package indicates that the binding data fit well to a two sequential sites model

accumulation of an intermediate state. The intermediate state is stable in the GdnHCl concentration range 2.20–2.40 M. Using a three-state (N ↔ I ↔ D) mechanism, we obtained the values of the thermodynamic parameters $\Delta G^0_{NI}$, $C^{NI}_m$, and $m_{NI}$ for the first transition (N ↔ I) and $\Delta G^*_{ID}$, $C^{ID}_m$, and $m_{ID}$ for the second transition (I ↔ D) of $Sr^{2+}$–ACF I by global analysis. According to Muzammil et al. [34], the value of $\Delta G^*_{ID}$ represents the value obtained from extrapolation of $\Delta G_{ID}$ values to the start of the process (I ↔ D), 2.3 M GdnHCl. As shown in Table 3, the $\Delta G^0_{total}$ of $Sr^{2+}$–ACF I in the presence of 1 mM $Sr^{2+}$, i.e., the free-energy change associated with the transformation of the native state to the intermediate state and finally to the denatured state, was calculated to be 5.85 ± 0.14 kcal/mol, which is greater than the $\Delta G^0$ of apo-ACF I (4.50 ± 0.08 kcal/mol) [16]. These results demonstrate that $Sr^{2+}$ ions markedly stabilize the conformation of ACF I.

Similarly, GdnHCl-induced denaturation of $Ba^{2+}$–ACF I is also a three-state process with a stable intermediate state. The intermediate state is stable in the GdnHCl concentration range 2.00–2.20 M. The total free energy change

**Table 1** Thermodynamic parameters for metal ion binding to $Ca^{2+}$-free anticoagulation factor I (apo-ACF I) at pH 7.6 obtained from isothermal titration calorimetry measurements in 20 mM tris(hydroxymethyl)aminomethane (Tris) at 25 °C

| Ligand | Site | $K_A$ ($M^{-1}$) | $\Delta G$ (kcal/mol) | $\Delta H$ (kcal/mol) | $\Delta S$ (cal/mol K) | $T\Delta S$ (kcal/mol) |
|---|---|---|---|---|---|---|
| $Ca^{2+}$ | I | $(1.26 \pm 0.29) \times 10^5$ | $-6.94 \pm 0.21$ | $-8.87 \pm 1.96$ | $-6.48 \pm 1.61$ | $-1.93 \pm 0.48$ |
| | II | $(1.01 \pm 0.12) \times 10^4$ | $-5.21 \pm 0.11$ | $-6.43 \pm 0.93$ | $-4.08 \pm 1.07$ | $-1.22 \pm 0.32$ |
| $Sr^{2+}$ | I | $(1.09 \pm 0.22) \times 10^5$ | $-6.87 \pm 0.13$ | $-9.60 \pm 1.74$ | $-9.17 \pm 1.46$ | $-2.73 \pm 0.44$ |
| | II | $(5.10 \pm 1.39) \times 10^3$ | $-5.06 \pm 0.15$ | $-7.19 \pm 1.05$ | $-7.15 \pm 2.13$ | $-2.13 \pm 0.64$ |
| $Ba^{2+}$ | I | $(5.91 \pm 1.45) \times 10^4$ | $-6.51 \pm 0.17$ | $-12.50 \pm 2.86$ | $-20.12 \pm 3.41$ | $-6.00 \pm 1.02$ |
| | II | $(4.12 \pm 0.90) \times 10^3$ | $-4.93 \pm 0.13$ | $-8.75 \pm 1.74$ | $-12.82 \pm 1.98$ | $-3.82 \pm 0.59$ |

All values represent the average of triplicate determinations

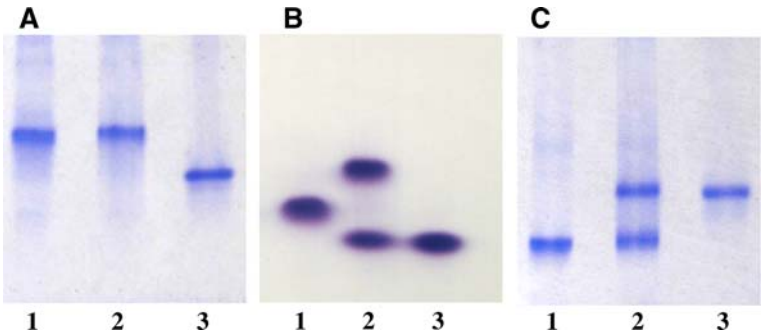


**Fig. 3** Analysis of the effects of metal ions on the binding of ACF I to activated coagulation factor X (FXa) by nondenaturing polyacrylamide gel electrophoresis. **a** Samples were electrophoresed in the presence of 1 mM $Mg^{2+}$. *Lane 1* contained 10 µl FXa; *lane 2* contained 5 µl apo-ACF I and 5 µl FXa; *lane 3* contained 10 µl apo-ACF I. **b** Samples were electrophoresed in the presence of 1 mM $Sr^{2+}$. *Lane 1* contained 10 µl FXa; *lane 2* contained 10 µl apo-ACF I and 5 µl FXa; *lane 3* contained 10 µl apo-ACF I. **c** Samples were electrophoresed in the presence of 1 mM $Ba^{2+}$. *Lane 1* contained 8 µl FXa; *lane 2* contained 8 µl apo-ACF I and 8 µl FXa; *lane 3* contained 8 µl apo-ACF I. The concentrations of both apo-ACF I and FXa were 20 µM

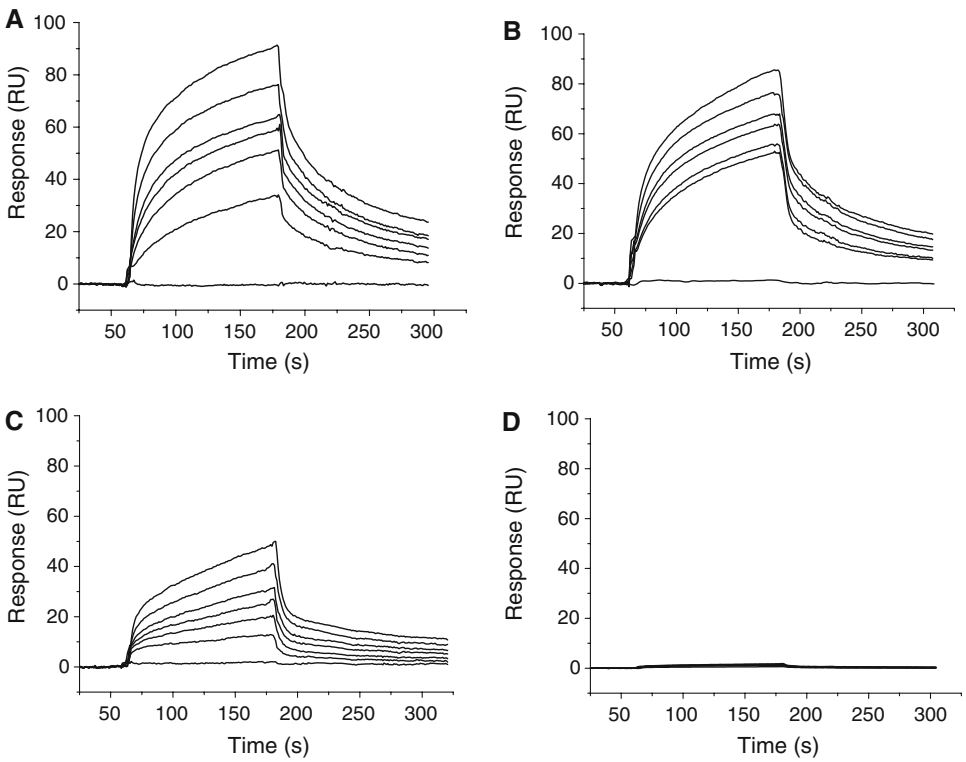


**Fig. 4** Surface plasmon resonance kinetic analysis of the effect of metal ions on the interaction of ACF I with FXa. Apo-ACF I in 0.02 M Tris–HCl (pH 7.6) containing 1 mM $Mg^{2+}$ (**a**), $Ca^{2+}$ (**b**), $Sr^{2+}$ (**c**), or $Ba^{2+}$ (**d**) was injected over an immobilized FXa surface at concentrations of 0, 0.31, 0.62, 1.2, 2.5, 5.0, and 10 $\mu$M for 2 min, and dissociation was monitored for 3 min. The kinetic parameters were obtained from each interaction by a fit of the data to a 1:1 Langmuir model

**Table 2** Effect of metal ions on kinetic parameters for binding of ACF I with FXa in 20 mM Tris (pH 7.6) determined by surface plasmon resonance

| Metal ion | $k_{on}$ ($M^{-1}$ $s^{-1}$) | $k_{off}$ ($s^{-1}$) | $K_A$ ($M^{-1}$) | $K_D$ (M) |
|---|---|---|---|---|
| $Mg^{2+}$ | $(1.4 \pm 0.3) \times 10^4$ | $(8.8 \pm 1.6) \times 10^{-3}$ | $(1.6 \pm 0.3) \times 10^6$ | $(6.2 \pm 0.9) \times 10^{-7}$ |
| $Ca^{2+}$ | $(1.8 \pm 0.2) \times 10^4$ | $(9.2 \pm 1.9) \times 10^{-3}$ | $(1.9 \pm 0.4) \times 10^6$ | $(5.3 \pm 1.2) \times 10^{-7}$ |
| $Sr^{2+}$ | $(4.9 \pm 0.7) \times 10^3$ | $(6.7 \pm 1.1) \times 10^{-3}$ | $(7.4 \pm 0.8) \times 10^5$ | $(1.4 \pm 0.2) \times 10^{-6}$ |

All values represent the average of triplicate determinations

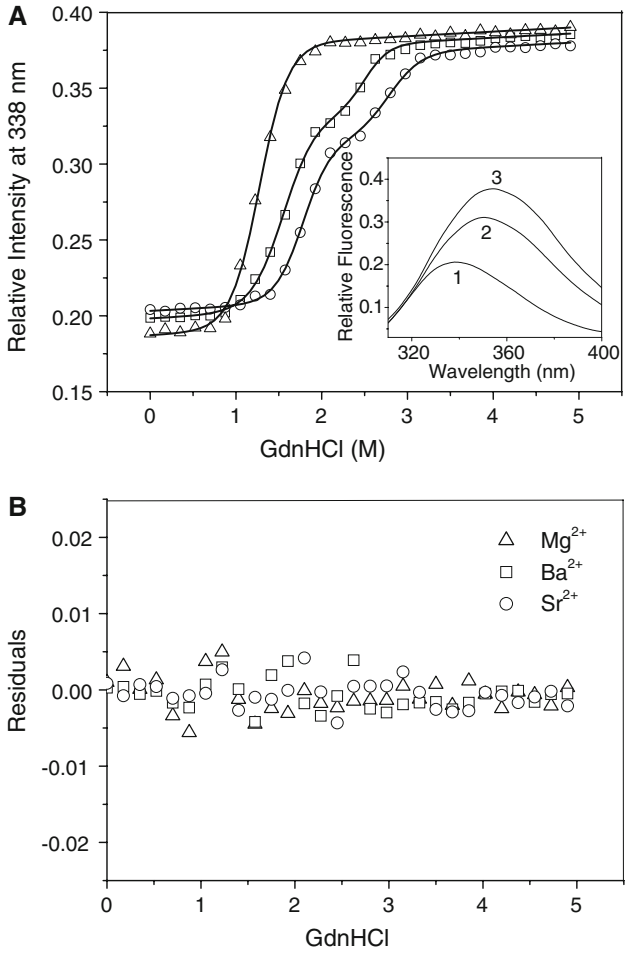


**Fig. 5** The effects of metal ions on guanidine hydrochloride (GdnHCl)-induced unfolding of ACF I in 0.02 M Tris–HCl buffer (pH 7.6, 25 °C). A protein concentration of 1 μM was used in the study. Unfolding transitions of apo-ACF I in the presence of 1 mM $Mg^{2+}$ (*triangles*), $Ba^{2+}$–ACF I in the presence of 1 mM $Ba^{2+}$ (*squares*), and $Sr^{2+}$–ACF I in the presence of 1 mM $Sr^{2+}$ (*circles*) were monitored by measurement of fluorescence at 338 nm after excitation at 295 nm. **a** The *curves* are the fitting curves based on experimental points by nonlinear least-squares analysis for a two-state transition of apo-ACF I in the presence of 1 mM $Mg^{2+}$ and by the global analysis for three-state transitions of $Ba^{2+}$–ACF I in the presence of 1 mM $Ba^{2+}$ and $Sr^{2+}$–ACF I in the presence of 1 mM $Sr^{2+}$. The *inset* depicts the intrinsic fluorescence spectra of $Sr^{2+}$–ACF I in the presence of 1 mM $Sr^{2+}$ in native (*1*), 2.3 M GdnHCl intermediate (*2*), and 4.9 M GdnHCl unfolded (*3*) states. **b** Residuals between the experimental and the theoretical data during GdnHCl-induced unfolding

(N ↔ I ↔ D) for $Ba^{2+}$–ACF I in the presence of 1 mM $Ba^{2+}$ is also greater than the $\Delta G^0$ of apo-ACF I (Table 3), suggesting that $Ba^{2+}$ ions also increase the conformational stability of ACF I.

Far-UV CD spectroscopy was also used to analyze the effects of metal ions on GdnHCl-induced unfolding of ACF I. As shown in Fig. 6, all transition profiles of apo-ACF I in the presence of 1 mM $Mg^{2+}$, $Sr^{2+}$–ACF I in the presence of 1 mM $Sr^{2+}$, and $Ba^{2+}$–ACF I in the presence of 1 mM $Ba^{2+}$ show a two-state process with no apparent intermediate state(s). Using a two-state mechanism, we obtained the $\Delta G^0$, $C_m$, and $m$ values for the three transition profiles and they are shown in Table 3.

The normalized transition curves for GdnHCl-induced unfolding of apo-ACF I in the presence of 1 mM $Mg^{2+}$ monitored by the measurements of ellipticity at 222 nm and fluorescence at 338 nm are nearly superimposable (data not shown). The $\Delta G^0$ (4.51 ± 0.10 kcal/mol) estimated from the far-UV ellipticity is similar to that determined by fluorescence spectroscopy (4.54 ± 0.09 kcal/mol). These results further suggest that $Mg^{2+}$ ions do not affect GdnHCl-induced unfolding of apo-ACF I.

The normalized transition curve for GdnHCl-induced unfolding of $Sr^{2+}$–ACF I monitored by the measurements of ellipticity at 222 nm and the normalized transition curve for the GdnHCl-induced first transition (N ↔ I) of $Sr^{2+}$–ACF I monitored by the fluorescence at 338 nm are nearly superimposable (data not shown), suggesting that the two-state transition of $Sr^{2+}$–ACF I monitored by the measurements of ellipticity at 222 nm corresponds to the first transition (N ↔ I) of $Sr^{2+}$–ACF I monitored by the fluorescence at 338 nm. The unfolding $\Delta G^0$ (4.79 ± 0.14 kcal/mol) estimated from the far-UV ellipticity is similar to $\Delta G^0_{NI}$ of the N ↔ I transition of $Sr^{2+}$–ACF I determined by fluorescence spectroscopy (4.73 ± 0.08 kcal/mol). However, the existence of the second unfolding transitions monitored by the fluorescence measurements, i.e., I ↔ D, was not detected by far-UV CD measurements. These results demonstrate that the unfolding intermediate state of $Sr^{2+}$–ACF I has extensive disordering of the native structures with little folding conformation being retained.

**Table 3** Thermodynamic parameters for unfolding equilibria of $Mg^{2+}$ + apo-ACF I, $Sr^{2+}$–ACF I, and $Ba^{2+}$–ACF I induced by GdnHCl at 25 °C, monitored by measurements of fluorescence at 338 nm and ellipticity at 222 nm

| Species | $C_m^{NI}$ (N ↔ I) (M) | $C_m^{ID}$ (I ↔ D) (M) | $m_{NI}$ (N ↔ I) (kcal/M mol) | $m_{ID}$ (I ↔ D) (kcal/M mol) | $\Delta G^0_{NI}$ (N ↔ I) (kcal/mol) | $\Delta G^*_{ID}$ (I ↔ D) (kcal/mol) | $\Delta G^0_{total}$ (N ↔ I ↔ D) (kcal/mol) |
|---|---|---|---|---|---|---|---|
| $Sr^{2+}$–ACF I[a] | 1.71 ± 0.03 | 2.75 ± 0.07 | 2.77 ± 0.03 | 3.51 ± 0.06 | 4.73 ± 0.08 | 1.12 ± 0.06 | 5.85 ± 0.14 |
| $Ba^{2+}$–ACF I[a] | 1.54 ± 0.03 | 2.50 ± 0.05 | 3.02 ± 0.06 | 3.64 ± 0.06 | 4.65 ± 0.10 | 0.97 ± 0.03 | 5.62 ± 0.13 |

| Species | $C_m$ (M) | $m$ (kcal/M mol) | $\Delta G^0$ (kcal/mol) |
|---|---|---|---|
| $Mg^{2+}$ + apo-ACF I[a] | 1.27 ± 0.02 | 3.56 ± 0.07 | 4.54 ± 0.09 |
| $Mg^{2+}$ + apo-ACF I[b] | 1.27 ± 0.03 | 3.54 ± 0.06 | 4.51 ± 0.10 |
| $Sr^{2+}$–ACF I[b] | 1.74 ± 0.07 | 2.76 ± 0.08 | 4.79 ± 0.14 |
| $Ba^{2+}$–ACF I[b] | 1.56 ± 0.04 | 2.96 ± 0.05 | 4.60 ± 0.08 |

All values represent the average of triplicate determinations

[a] The values were monitored by measurements of the fluorescence at 338 nm

[b] The values were monitored by measurements of ellipticity at 222 nm

The normalized transition curve for GdnHCl-induced unfolding of $Ba^{2+}$–ACF I monitored by the measurements of ellipticity at 222 nm and the normalized transition curve for the GdnHCl-induced first transition (N ↔ I) of $Ba^{2+}$–ACF I monitored by the fluorescence at 338 nm are nearly superimposable (data not shown), suggesting that the two-state transition of $Ba^{2+}$–ACF I monitored by the measurements of ellipticity at 222 nm corresponds to the first transition (N ↔ I) of $Ba^{2+}$–ACF I monitored by the fluorescence at 338 nm. The unfolding $\Delta G^0$ (4.79 ± 0.14 kcal/mol) estimated from the far-UV ellipticity is similar to $\Delta G^0_{NI}$ of the N ↔ I transition of $Ba^{2+}$–ACF I determined by fluorescence spectroscopy (4.73 ± 0.08 kcal/mol). However, the existence of the second unfolding transitions monitored by the fluorescence measurements, i.e., I ↔ D, was also not detected by far-UV CD measurements. These results indicate that the unfolding intermediate state of $Ba^{2+}$–ACF I also has extensive disordering of the native structures with little folding conformation being retained.

### Metal-ion-induced partial refolding of ACF I

We have shown that $Ca^{2+}$ ions are able to induce a partial refolding of apo-ACF I from the unfolded state to the intermediate state with two folding populations. It is obvious from Fig. 5 that in the GdnHCl concentration range 2.1–2.3 M apo-ACF I is in the denatured state, while $Sr^{2+}$–ACF I and $Ba^{2+}$–ACF I are in the intermediate state. Therefore, it might be possible to perform a partial refolding jump from the unfolded state of apo-ACF I to the intermediate state of $Sr^{2+}$–ACF I or $Ba^{2+}$–ACF I by adding $Sr^{2+}$ or $Ba^{2+}$ ions. Such transitions could be monitored by fluorescence measurements. The intrinsic fluorescence intensity of apo-ACF I began to decrease after addition of 1 mM $Sr^{2+}$ or $Ba^{2+}$ to the unfolded apo-ACF I at 2.3 M or 2.1 M GdnHCl concentration. The quenching of Trp fluorescence by $Sr^{2+}$ or $Ba^{2+}$ reflects the formation of compact metal-binding regions, suggesting metal-ion-induced partial refolding of the protein.

The partial refolding kinetics was monitored by Trp fluorescence at 338 nm after addition of metal ions to the unfolded apoprotein. Figure 7 shows representative kinetic traces. The kinetics of $Sr^{2+}$-induced partial refolding monitored by Trp fluorescence at 338 nm could not be satisfactorily fit to a single-exponential function. A sum of two-exponential terms best fits the partial refolding curve, yielding rate constant values of 3.28 ± 0.04 and 0.91 ± 0.01 $min^{-1}$ for the faster and slower phases, respectively. The kinetics of $Ba^{2+}$-induced partial refolding was also best fit to a sum of two-exponential terms yielding rate constant values of 0.381 ± 0.005 and 0.118 ± 0.002 $min^{-1}$ for the faster and slower phases, respectively.

## Discussion

The goal of the present study was to characterize the thermodynamics of metal ion binding to ACF I as well as to analyze the effects of metal ion substitutions in ACF I on the structural stability and the binding affinity for FXa. A metal ionic radius dependent effect was found in the affinities for the binding of ACF I to alkaline earth metal ions. ACF I can bind with two $Sr^{2+}$ or two $Ba^{2+}$ ions, but only $Sr^{2+}$ ions support the binding of ACF I to FXa. Previous studies showed that $Sr^{2+}$ ions can be substituted for $Ca^{2+}$ ions in IX/X-bps only in their binding of FIX [2, 4]. This is first time it has been shown that $Sr^{2+}$ ions are also able to substitute $Ca^{2+}$ ions in the binding of ACF I to FXa. Although $Mg^{2+}$ ions show significantly low affinity for

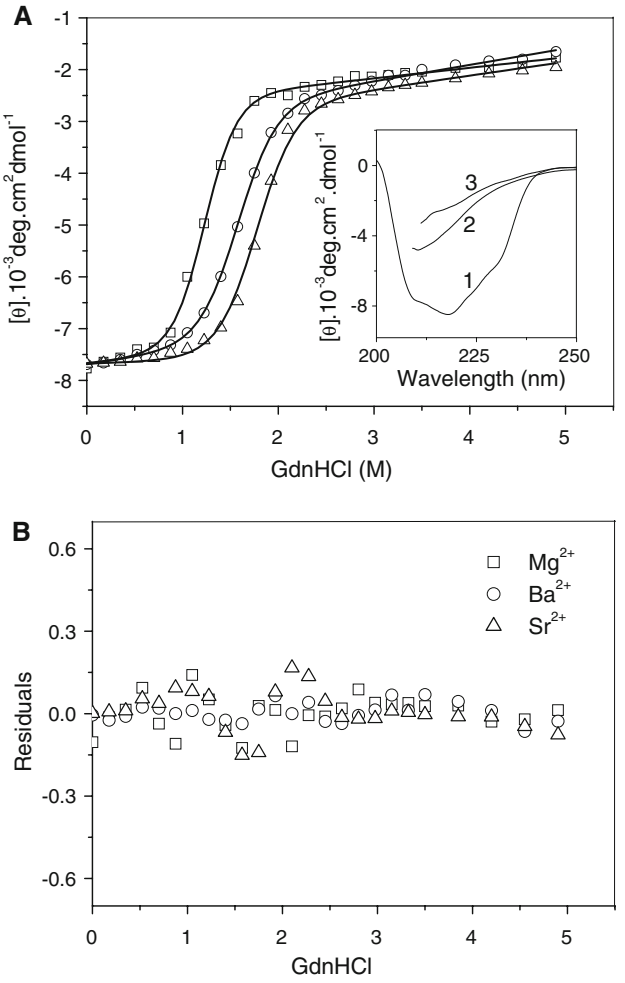


**Fig. 6** GdnHCl-induced changes of the far-UV circular dichroism (CD) spectra of ACF I in 0.02 M Tris–HCl buffer, pH 7.6, 25 °C. The protein concentration was 0.10 mg/ml. **a** Changes in far-UV CD ellipticity at 222 nm of apo-ACF I in the presence of 1 mM $Mg^{2+}$ (*squares*), $Sr^{2+}$–ACF I in the presence of 1 mM $Sr^{2+}$ (*triangles*), and $Ba^{2+}$–ACF I in the presence of 1 mM $Ba^{2+}$ (*circles*). The *curves* are the fitting curves based on experimental points by nonlinear least-squares analysis. The *inset* shows the far-UV CD spectra of $Sr^{2+}$–ACF I in the native (*1*), 2.3 M GdnHCl intermediate (*2*), and 4.9 M GdnHCl unfolded (*3*) states. **b** Residuals between the experimental and the theoretical data during GdnHCl-induced unfolding

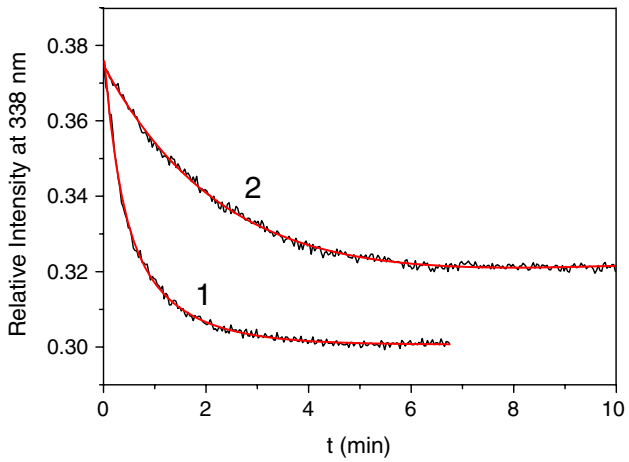


**Fig. 7** Metal-ion-induced partial refolding of apo-ACF I from the unfolded state to the intermediate state in 0.02 M Tris–HCl buffer (pH 7.6), monitored by measurement of fluorescence at 338 nm by excitation at 295 nm. Partial refolding was initiated by adding 1 mM $Sr^{2+}$ to 1 μM apo-ACF I in 2.3 M GdnHCl (*1*) or by adding 1 mM $Ba^{2+}$ to 1 μM apo-ACF I in 2.1 M GdnHCl (*2*). Both *red curves* were obtained after fitting to a sum of two-exponential terms based on experimental curves (*black curves*)

binding to apo-ACF I, $Mg^{2+}$ ions also induce the binding of ACF I with FXa.

The $Mg^{2+}$ ion has a too small ionic radius compared with the $Ca^{2+}$ ion and probably does not match the $Ca^{2+}$-specific sites in ACF I, which should be the reason why $Mg^{2+}$ has a low binding affinity for ACF I. As shown in Fig. 1, each $Ca^{2+}$-binding site in ACF I locates within a helix–loop–sheet domain which is different from the classic EF-hand $Ca^{2+}$-binding motif that comprises a helix–loop–helix domain [40]. The proteins in the EF-hand family usually have two high-affinity $Ca^{2+}$–$Mg^{2+}$ sites and two low affinity $Ca^{2+}$-specific sites [41]; however, ACF I has two high-affinity $Ca^{2+}$–$Sr^{2+}$ sites that show slightly low affinity for $Ba^{2+}$ and much lower affinity for $Mg^{2+}$.

It has been reported that *Deinagkistrodon* X-bp from *Deinagkistrodon* venom binds with the Gla domain of FX [10]. ACF I has an amino acid sequence highly similar to that of *Deinagkistrodon* X-bp, with only residue Asn-70 in the *β* chain of ACF I being replaced by Lys-70 in *Deinagkistrodon* X-bp [15]. It is therefore reasonable to assume that ACF I also binds with the Gla domain in FXa. FXa is a $Ca^{2+}$- and $Mg^{2+}$-binding protein with multiple $Ca^{2+}$- and $Mg^{2+}$-binding sites in its Gla domain [42, 43]. The Gla domain is responsible for $Ca^{2+}$-dependent phospholipid membrane binding [10]. $Sr^{2+}$ ions can replace $Ca^{2+}$ ions in FX for inducing FX to bind the phospholipid membrane [44]. The binding of $Mg^{2+}$, $Ca^{2+}$, and $Sr^{2+}$ ions to FXa might be essential for the recognition between FXa and ACF I. SPR spectroscopy shows that ACF I has a similar binding affinity for FXa in the presence of 1 mM $Mg^{2+}$ compared with that in the presence of 1 mM $Ca^{2+}$ (Table 2). In blood plasma, free $Mg^{2+}$ ion is present in relatively high concentrations (0.4–0.6 mM) [45]. The abundant $Mg^{2+}$ in blood may play a role in the anticoagulation of ACF I. Although $Ba^{2+}$ can bind to ACF I, $Ba^{2+}$ cannot induce the binding of ACF I to FXa, suggesting that the binding of $Ba^{2+}$ to ACF I is not essential for the interaction of ACF I with FXa. Our recent data show that the mobility of FXa in native PAGE is greater than that of ACF I in the absence of metal ions. When FXa binds with multiple $Ca^{2+}$ ions in the presence of 1 mM $Ca^{2+}$, its mobility markedly decreases and is less than that of $Ca^{2+}$–ACF I. Figure 3a and b shows that when FXa

binds with multiple $Mg^{2+}$ or $Sr^{2+}$ ions in the presence of 1 mM $Mg^{2+}$ or $Sr^{2+}$, its mobility is less than that of ACF I. The greater mobility of FXa in the presence of 1 mM $Ba^{2+}$ than that of $Ba^{2+}$–ACF I (Fig. 3c) suggests that FXa cannot bind with $Ba^{2+}$, which may be the reason why $Ba^{2+}$ cannot support the binding of ACF I with FXa.

$Ca^{2+}$ ions were found to increase the structural stability of ACF I [16]. As shown in Fig. 1, the N-terminal region of the second α-helix in the A chain is tightly associated with the C-terminal tail in the same chain via one $Ca^{2+}$; similarly, the N-terminal region of the second α-helix in the B chain is also tightly associated with the C-terminal tail in the same chain via another $Ca^{2+}$. $Ca^{2+}$ ions act to fasten the protein structure as a lock. $Ca^{2+}$-induced rigidification of ACF I should contribute to the negative $\Delta S$ values for both $Ca^{2+}$ binding interactions (Table 1). A similar result has been reported for habu IX/X-bp, which undergoes a conformational change from a loose, amorphous conformation to a rigid, ordered conformation upon binding of $Ca^{2+}$ ions [46].

The alkaline earth metal ions $Mg^{2+}$, $Ca^{2+}$, $Sr^{2+}$, and $Ba^{2+}$ are hard acids with the same positive charge, but they have different ionic radii: 0.078, 0.106, 0.127, and 0.143 nm, respectively (http://www.chemsoc.org). The equilibrium dialysis result shows that the smallest of these alkaline earth metal cations, $Mg^{2+}$, with an ionic radius less than that of $Ca^{2+}$, has significantly low binding affinity for apo-ACF I. In contrast, the bigger alkaline earth metal cations, $Sr^{2+}$ and $Ba^{2+}$, with radii larger than the ionic radius of $Ca^{2+}$, can occupy the two $Ca^{2+}$ sites in ACF I, which is further confirmed by ITC measurements (Fig. 2). The ionic radius of $Sr^{2+}$ is most similar to that of $Ca^{2+}$ among the alkaline earth metal ions, and as a result, the thermodynamic parameters ($K_A$, $\Delta G$, $\Delta H$, and $\Delta S$) for $Sr^{2+}$ binding in both sites obtained by ITC are slightly different from those for $Ca^{2+}$ binding (Table 1). The value of $K_{A1}$, i.e., $(1.09 \pm 0.22) \times 10^5$ $M^{-1}$, is very similar to that for $Ca^{2+}$ binding, i.e., $(1.26 \pm 0.29) \times 10^5$ $M^{-1}$. The similarity in the ionic radii of $Sr^{2+}$ and $Ca^{2+}$ should be the reason why $Sr^{2+}$ ions can substitute $Ca^{2+}$ ions in both ACF I and FXa for inducing the interaction between the two proteins (Figs. 3, 4) [44]. In contrast, the ionic radius of $Ba^{2+}$ is much larger than that of $Ca^{2+}$, and as a result, the thermodynamic parameters for $Ba^{2+}$ binding in both sites ($K_A$, $\Delta G$, $\Delta H$, and $\Delta S$) obtained by ITC are very different from those for $Ca^{2+}$ binding (Table 1). The obvious decreases in both $K_{A1}$ and $K_{A2}$ after the substitution of $Ba^{2+}$ for $Ca^{2+}$ indicate that the $Ca^{2+}$-specific sites have low affinity for $Ba^{2+}$ ion. These results indicate that the $Ca^{2+}$-binding sites in ACF I select metal ions on the basis of ion size.

Another intriguing observation in the study is that the radii of metal ions affect the structural stability of ACF I. The replacement of $Ca^{2+}$ by $Sr^{2+}$ or $Ba^{2+}$ affects the unfolding $\Delta G^0_{total}$ of the protein. A comparison of the free-energy changes for $Ca^{2+}$–ACF I, $Sr^{2+}$–ACF I, and $Ba^{2+}$–ACF I during GdnHCl-induced unfolding monitored by fluorescence spectroscopy clearly indicates that the $\Delta G^0_{total}$ of $Sr^{2+}$–ACF I is slightly less than the $\Delta G^0_{total}$ of $Ca^{2+}$–ACF I and the difference is $0.16 \pm 0.14$ kcal/mol, while the $\Delta G^0_{total}$ of $Ba^{2+}$–ACF I is much less than the $\Delta G^0_{total}$ of $Ca^{2+}$–ACF I and the difference is $0.39 \pm 0.13$ kcal/mol. The result suggests that $Sr^{2+}$-stabilized ACF I exhibits slightly lower resistance to GdnHCl denaturation than $Ca^{2+}$–ACF I, while $Ba^{2+}$-stabilized ACF I exhibits much lower resistance to GdnHCl denaturation than $Ca^{2+}$–ACF I. The ionic radius of $Sr^{2+}$ is similar to that of $Ca^{2+}$; thus, the substitution of $Sr^{2+}$ for $Ca^{2+}$ has relatively little effect on the stability of ACF I. The ionic radius of $Ba^{2+}$ is much larger than that of $Ca^{2+}$; therefore, the substitution of $Ba^{2+}$ for $Ca^{2+}$ has a relatively large effect on the stability of ACF I.

The first transitions (N ↔ I) of $Sr^{2+}$–ACF I and $Ba^{2+}$–ACF I monitored by the fluorescence at 338 nm were confirmed by the measurements of ellipticity at 222 nm; however, the existence of their second unfolding transitions (I ↔ D) monitored by the fluorescence measurements is not detectable by far-UV CD measurements. The intermediate states of $Sr^{2+}$–ACF I and $Ba^{2+}$–ACF I seem to have following characteristics: (1) the loss of native structure, according to the significant increase of intrinsic fluorescence intensity from the native state to the I state; (2) the loss of most of the secondary structure as indicated by a marked change of far-UV CD spectra from the native state to the intermediate state; (3) the retention of little folding conformation within local hydrophobic regions, as judged from the second transition from the unfolding of the intermediate state to the denatured state of $Sr^{2+}$–ACF I or $Ba^{2+}$–ACF I resulting in a further increase of fluorescence intensity by 17 or 15% with a redshift of $\lambda_{max}$ from 350 to 354 nm; (4) the exposure of the most Trp residues, based on the significant redshift of the intrinsic fluorescence from the native state to the intermediate state. Comparison of the intermediate state characteristics of $Sr^{2+}$–ACF I or $Ba^{2+}$–ACF I with those of $Ca^{2+}$–ACF I indicates that the intermediate state of $Sr^{2+}$–ACF I or $Ba^{2+}$–ACF I corresponds to the second intermediate state of $Ca^{2+}$–ACF I [16].

Interestingly, by comparing the denaturation profiles of apo-ACF I, $Sr^{2+}$–ACF I, and $Ba^{2+}$–ACF I monitored by the fluorescence measurements, we found that under appropriate denaturing condition (2.1–2.3 M GdnHCl), a partial refolding jump could be initiated. Indeed, we were able to initiate partial refolding of unfolded apo-ACF I simply by adding 1 mM $Sr^{2+}$ or 1 mM $Ba^{2+}$. Fluorescence measurements show that the partial refolding process from the unfolded state of apo-ACF I to the intermediate state of

$Sr^{2+}$–ACF I or $Ba^{2+}$–ACF I is best fit by a sum of two exponential terms, suggesting a faster and a slower partial folding population in both processes (Fig. 7), as observed for $Ca^{2+}$-induced partial refolding of the protein [16]. A previous study showed that the faster step involves the formation of the compact metal-binding site regions [16]. Subsequently, the protein undergoes further conformational rearrangements, which corresponds to the second step to form the global structure of the intermediate state as observed from the further decrease of the intrinsic fluorescence. It is interesting to note that the refolding rate constant value ($3.28 \pm 0.04$ $min^{-1}$) of the faster phase for the process of $Sr^{2+}$-induced partial refolding is less than that ($5.49 \pm 0.07$ $min^{-1}$) of the faster phase for the process of $Ca^{2+}$-induced partial refolding, but the refolding rate constant value ($0.91 \pm 0.01$ $min^{-1}$) of the slower phase for the process of $Sr^{2+}$-induced partial refolding is very similar to that ($0.90 \pm 0.01$ $min^{-1}$) of the slower phase for the process of $Ca^{2+}$-induced partial refolding [16]. The substitution of $Ba^{2+}$ ions for $Ca^{2+}$ ions significantly decreases both the faster and the slower partial refolding rate constants from $5.49 \pm 0.07$ to $0.381 \pm 0.005$ $min^{-1}$ and from $0.90 \pm 0.01$ to $0.118 \pm 0.002$ $min^{-1}$, respectively. Although we cannot infer the detailed picture of the pathway of the metal-ion-induced partial refolding from the present data, it is certain that the metal-ion-induced partial refolding of apo-ACF I could be performed without changing the concentration of the denaturant.

## Conclusions

The ionic radii of the cations occupying $Ca^{2+}$-binding sites in ACF I crucially affect the binding affinity of ACF I for alkaline earth metal ions as well as the structural stability of ACF I against GdnHCl denaturation. $Sr^{2+}$ and $Ba^{2+}$, with ionic radii larger than the ionic radius of $Ca^{2+}$, can bind to apo-ACF I, while $Mg^{2+}$, with an ionic radius smaller than that of $Ca^{2+}$, shows significantly low affinity for the binding to apo-ACF I. All bindings of $Ca^{2+}$, $Sr^{2+}$, and $Ba^{2+}$ ions in two sites of ACF I are mainly enthalpy-driven and the entropy is unfavorable for them. $Mg^{2+}$ and $Sr^{2+}$, with ionic radii similar to the ionic radius of $Ca^{2+}$, can bind to FXa and therefore also induce the binding of ACF I to FXa, whereas $Ba^{2+}$, with a much larger ionic radius than that of $Ca^{2+}$, cannot support the binding of ACF I with FXa. Our observations suggest that bindings of $Ca^{2+}$, $Sr^{2+}$, and $Ba^{2+}$ ions in two sites of ACF I increase the structural stability of ACF I, but these bindings are not essential for the binding of ACF I with FXa, and that the binding of $Mg^{2+}$, $Ca^{2+}$, and $Sr^{2+}$ ions to FXa may be essential for the recognition between FXa and ACF I.

**Acknowledgments** We are grateful for financial support from the National Natural Science Foundation of China (grants no. 20871111, 20571069, 20171041).

## References

1. Jackson CM, Nemerson Y (1980) Annu Rev Biochem 49:765–811
2. Sekiya F, Atoda H, Morita T (1993) Biochemistry 32:6892–6897
3. Atoda H, Ishikawa M, Yoshihara E, Sekiya F, Morita T (1995) J Biochem 118:965–973
4. Chen YL, Tsai IH (1996) Biochemistry 35:5264–5271
5. Atoda H, Ishikawa M, Mizuno H, Morita T (1998) Biochemistry 37:17361–17370
6. Gopinath SCB, Shikamoto Y, Mizuno H, Kumar PKR (2007) Biochem J 405:351–357
7. Zang JY, Teng MK, Niu LW (2003) Acta Crystallogr Sect D Biol Crystallogr 59:730–733
8. Lee WH, Zhuang QY, Zhang Y (2003) Toxicon 41:765–772
9. Morita T (2005) Toxicon 45:1099–1114
10. Mizuno H, Fujimoto Z, Atoda H, Morita T (2001) Proc Natl Acad Sci USA 98:7230–7234
11. Mizuno H, Fujimoto Z, Koizumi M, Kano H, Atoda H, Morita T (1997) Nat Struct Biol 4:438–441
12. Mizuno H, Fujimoto Z, Koizumi M, Kano H, Atoda H, Morita T (1999) J Mol Biol 289:103–112
13. Xu XL, Liu QL, Xie YS, Wu SD (2000) Toxicon 38:1517–1528
14. Xu XL, Liu QL (2001) Toxicon 39:1359–1365
15. Hu SY, Li WF, Chen L, Liu J (2005) Toxicon 46:716–724
16. Xu XL, Liu QL, Yu HM, Xie YS (2002) Protein Sci 11:944–956
17. Deng NJ, Yan L, Singh D, Cieplak P (2006) Biophys J 90:3865–3879
18. Yoon T, Dizin E, Cowan JA (2007) J Biol Inorg Chem 12:535–542
19. Miras R, Morin I, Jacquin O, Cuillel M, Guillain F, Mintz E (2008) J Biol Inorg Chem 13:195–205
20. Hou ZJ, Mitra B (2003) J Biol Chem 278:28455–28461
21. Ono T, Rompel A, Mino H, Chiba N (2001) Biophys J 81:1831–1840
22. Liu JB, Dutta SJ, Stemmler AJ, Mitra B (2006) Biochemistry 45:763–772
23. Prasad A, Pedigo S (2005) Biochemistry 44:13692–13701
24. Marlatt NM, Shaw GS (2007) Biochemistry 46:7478–7487
25. Golynskiy MV, Davis TC, Helmann JD, Cohen SM (2005) Biochemistry 44:3380–3389
26. Sujak A, Sanghamitra NJM, Maneg O, Ludwig B, Mazumdar S (2007) Biophys J 93:2845–2851
27. Yamniuk AP, Vogel HJ (2005) Protein Sci 14:1429–1437
28. Yamniuk AP, Silver DM, Anderson KL, Martin SR, Vogel HJ (2007) Biochemistry 46:7088–7098
29. Chalton DA, Kelly IF, McGregor A, Ridley H, Watkinson A, Miller J, Lakey JH (2007) Arch Biochem Biophys 465:1–10
30. Nielsen AD, Fuglsang CC, Westh P (2003) Biochem J 373:337–343
31. Smith CK, Windsor WT (2007) Biochemistry 46:1358–1367
32. Manak MS, Ferl RJ (2007) Biochemistry 46:1055–1063
33. Nozaki Y, Hirs CHW, Serge NT (1972) Methods in enzymology. Academic Press, New York, pp 43–50
34. Muzammil S, Kumar Y, Tayyab S (2000) Proteins Struct Funct Genet 40:29–38
35. Pace CN (1990) Trends Biotechnol 8:93–98
36. Xu XL, Liu QL, Xie YS (2002) Biochemistry 41:3546–3554
37. Ionescu RM, Smith VF, O'Neill JC, Matthews CR (2000) Biochemistry 39:9540–9550

38. Duy C, Fitter J (2006) Biophys J 90:3704–3711
39. Gross E, Peng DQ, Hazen SL, Smith JD (2006) Biophys J 90:1362–1370
40. Houdusse A, Love ML, Dominguez R, Grabarek Z, Cohen C (1997) Structure 5:1695–1711
41. Gopal B, Swaminathan CP, Bhattacharya S, Bhattacharya A, Murthy MRN, Surolia A (1997) Biochemistry 36:10910–10916
42. Persson E, Ostergaard A (2007) J Thromb Haemost 5:1977–1978
43. Sunnerhagen M, Olah GA, Stenflo J, Forsen S, Drakenberg T, Trewhella J (1996) Biochemistry 35:11547–11559
44. Nelsestuen GL, Broderius M, Martin G (1976) J Biol Chem 251:6886–6893
45. Shikamoto Y, Morita T, Fujimoto Z, Mizuno H (2003) J Biol Chem 278:24090–24094
46. Mizuno H, Atoda H, Morita T (1991) J Mol Biol 220:225–226